The effect of a C298D mutation in CaHydA [FeFe]-hydrogenase: Insights into the protein-metal cluster interaction by EPR and FTIR spectroscopic investigation

Title:

The effect of a C298D mutation in CaHydA [FeFe]-hydrogenase: insights into the protein-metal cluster interaction by EPR and FTIR spectroscopic investigation.

Authors:

Simone Morra,[a] Sara Maurelli,[b] Mario Chiesa,[b] David W. Mulder,[c] Michael W. Ratzloff,[c] Elio Giamello,[b] Paul W. King,[c] Gianfranco Gilardi,[a] and Francesca Valetti[a,*]

[a] Department of Life Sciences and Systems Biology, University of Torino, Torino 10133, Italy.

[b] Department of Chemistry, University of Torino, Torino 10133, Italy.

[c] Biosciences Center, National Renewable Energy Laboratory, Golden, Colorado 80401, USA.

*Corresponding Author: francesca.valetti@unito.it

Abstract

A conserved cysteine located in the signature motif of the catalytic center (H-cluster) of [FeFe]-hydrogenases functions in proton transfer. This residue corresponds to C298 in *Clostridium acetobutylicum* CaHydA. Despite the chemical and structural difference, the mutant C298D retains fast catalytic activity, while replacement with any other aminoacid causes significant activity loss. Given the proximity of C298 to the H-cluster, the effect of the C298D mutation on the catalytic center was studied by continuous wave (CW) and pulse electron paramagnetic resonance (EPR) and by Fourier transform infrared (FTIR) spectroscopies.

Comparison of the C298D mutant with the *wild type* CaHydA by CW and pulse EPR showed that the electronic structure of the center is not altered. FTIR spectroscopy confirmed that absorption peak values observed in the mutant are virtually identical to those observed in the *wild type*, indicating that the H-cluster is not generally affected by the mutation. Significant differences were observed only in the inhibited state H_{ox}-CO: the vibrational modes assigned to the CO_{exo} and Fe_d-CO in this state are shifted to lower values in C298D, suggesting different interaction of these ligands with the protein moiety when C298 is changed to D298. More relevant to the catalytic cycle, the redox equilibrium between the H_{ox} and H_{red} states is modified by the mutation, causing a prevalence of the oxidized state.

This work highlights how the interactions between the protein environment and the H-cluster, a dynamic closely interconnected system, can be engineered and studied in the perspective of designing bio-inspired catalysts and mimics.

Keywords

[FeFe]-hydrogenase; proton transfer; EPR; HYSCORE; FTIR.

1. Introduction:

[FeFe]-hydrogenases are the redox enzymes that catalyze the reversible reaction $2H^+ + 2e^- \rightleftarrows H_2$ at high turnover rates. These enzymes are crucial in the biological production of hydrogen gas [1-3], a valuable fuel and an important intermediate in various industrial processes [4,5].

The main aim of this work is to investigate the effects of the C298D mutation on the spectroscopic features of *Clostridium acetobutylicum* [FeFe]-hydrogenase I (CaHydA), in order to analyse the consequences on the catalytic site caused by protein modifications in its proximity.

The catalytic site of [FeFe]-hydrogenases is an organometallic center named the H-cluster (Fig. 1); it is extremely peculiar for this class of enzymes and its unique chemical makeup requires a complex biosynthetic mechanism by specialized protein maturases [6-10]. The H-cluster is composed of two sub-clusters: a cubane [4Fe-4S] coordinated by four conserved protein cysteines that is bridged to a [2Fe] sub-cluster via one of these residues (Fig. 1) [11,12]. The [2Fe] sub-cluster is composed of two iron atoms, the proximal (Fe_p) and the distal (Fe_d), coordinated by non-protein ligands that are two terminal CO, a bridging CO and two terminal CN [11,13,14]. The two Fe atoms are also bridged by an organic ligand which was identified as a di(thiomethyl)amine [1,15-18].

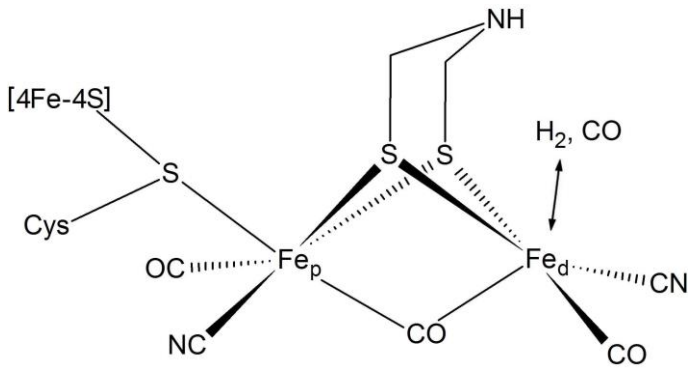

Figure 1. Structure of the H-cluster. **(Single column fitting image).**

The catalytic mechanism of H_2 evolution is based on the reduction of protons at Fe_d of the H-cluster, involving an hydride intermediate, but the details of the mechanism are still being investigated [19-24].

Several redox states of the H-cluster have been identified. The oxidized state (H_{ox}) is characterized by a diamagnetic $[4Fe\text{-}4S]^{2+}$ sub-cluster and a paramagnetic Fe(I)-Fe(II) sub-cluster. A one electron reduction results in the reduced state (H_{red}), characterized by a diamagnetic $[4Fe\text{-}4S]^{2+}$ sub-cluster and a diamagnetic Fe(I)-Fe(I) sub-cluster. A further one electron reduction results in the super-reduced state (H_{sred}), characterized by a paramagnetic $[4Fe\text{-}4S]^{1+}$ sub-cluster and a diamagnetic

Fe(I)-Fe(I) sub-cluster. A paramagnetic state $[4Fe\text{-}4S]^{1+}$ Fe(II)-Fe(II) diferrous intermediate has also been recently proposed [21]. Alternatively, binding of exogenous CO to the H_{ox} state at the Fe_d results in the reversibly inhibited form H_{ox}-CO, characterized by a diamagnetic $[4Fe\text{-}4S]^{2+}$ sub-cluster and a paramagnetic Fe(I)-Fe(II) sub-cluster [3,20,25-27].

Electron paramagnetic resonance (EPR) and Fourier transform infrared (FTIR) spectroscopies have been used for the characterisation of such intermediates because of their complementarity in the investigation of the electronic structure and the chemical environment of the different redox states of the H-cluster. Also, these spectroscopies have been used on [FeFe]-hydrogenases from different microorganisms, allowing the study of the similarities and the differences between different enzymes [3,25].

EPR and the related hyperfine techniques of ENDOR (electron nuclear double resonance) and HYSCORE (Hyperfine Sublevel Correlation) have proven to be powerful tools to elucidate the structure-function relationships of [FeFe]-hydrogenases. The EPR investigation has been focused on the paramagnetic states of the catalytic cycle namely the H_{ox} state and the H_{sred} state of algal enzymes (*Chlamydomonas reinhardtii*). The H_{sred} state, which has been proposed to be part of the catalytic cycle, displays a $[4Fe\text{-}4S]^{1+}$ Fe(I)Fe(I) configuration, with an EPR spectrum typical for a reduced $[4Fe\text{-}4S]^{1+}$ cluster [19]. By studying the hyperfine interactions of the ^{57}Fe nuclei of the cluster-core as well as the ^{14}N and ^{13}C nuclei belonging to the ligands, important insights were obtained on the spin density distribution and electronic structure of the H-cluster [3,17,28,29]. Moreover, the CO inhibited state of the enzyme, H_{ox}-CO, which is paramagnetic, yielded additional information on the redistribution of spin density in the H-cluster upon binding a π-accepting ligand in the exchangeable site at the distal iron [30].

FTIR spectroscopy was crucial in the identification of the non-protein CO and CN ligands in the H-cluster [31,32]. Subsequently, it has become a powerful specific tool to study how the redox state influences such ligands [19,20,23,33-35], their source during the assembly process [36] and the effect of mutagenesis [21,37].

The protein environment around the H-cluster was shown to be highly conserved in the entire enzyme class [1,26]. One of these strictly conserved residues is a cysteine that is adjacent to the Fe_d, namely C298 in *Clostridium acetobutylicum* HydA, C299 in *Clostridium pasteurianum* CpI and C169 in *Chlamydomonas reinhardtii* HydA1; its role in [FeFe]-hydrogenases has been investigated by means of X-ray crystallography [11], mutagenesis [21,37-40] and computational simulations [21,41,42].

In particular, we have previously shown [40] by site saturation mutagenesis that replacement of C298 in *Clostridium acetobutylicum* [FeFe]-hydrogenase (CaHydA) with any other aminoacid

causes severe impairment or loss of activity, with the only exception being aspartic acid. The mutant C298D, where the –SH group of cysteine was replaced by the –COOH group of aspartic acid in the proximity of the di(thiomethyl)amine bridge of H-cluster (Fig. 2), displays an enzymatic activity in the same order of magnitude of the *wild type* (WT), with only a 2-fold decrease in both H_2 evolution and H_2 uptake kinetics. Also, the activity pH profile was shifted towards acidic values. These data demonstrated a direct involvement of C298 in the proton transfer to the H-cluster.

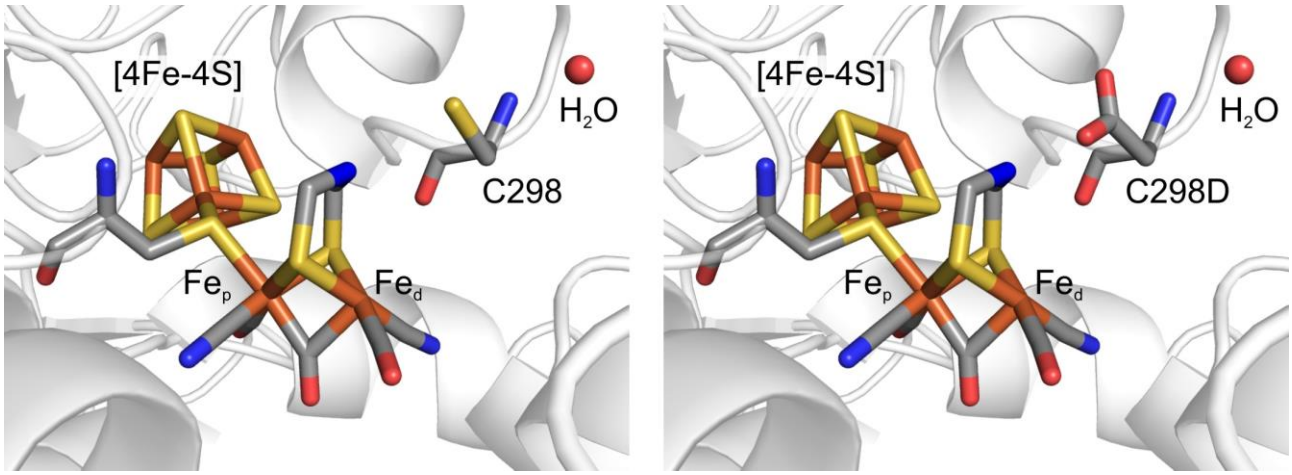

Figure 2. The H-cluster in a model of the protein environment of *Clostridium acetobutylicum* CaHydA [FeFe]-hydrogenase [40]. The structural position of the *wild type* cysteine 298 (C298) is depicted on the left, and the effect of the C298D mutation is modeled on the right. **(2 columns fitting image).**

In this work, we report a combination of continuous wave (CW) EPR, pulse EPR and FTIR spectroscopies that was used to compare CaHydA *wild type* (WT) to the C298D mutant to investigate, in detail, the effect of the mutation on the H-cluster structure under steady-state conditions of various redox states and its implications for catalysis.

2. Materials and methods:

2.1 Recombinant expression and purification

CaHydA WT and C298D were recombinantly expressed in *E. coli* by adapting previously described protocols [40,43-45]. The plasmids pCaE2 (harbouring the genes *hydA* and *hydE*) and pCaFG (harbouring the genes *hydF* and *hydG*) were co-transformed in *E. coli* Rosetta2(DE3). Cultures were aerobically grown in Terrific Broth medium supplemented with 2 mM ferric ammonium citrate, 200 µg/mL carbenicillin, 50 µg/uL streptomycin and 34 µg/mL chloramphenicol. When the OD_{600} reached ~0.4, the culture was supplemented with 2 mM cysteine, 25 mM fumarate, 0.5 % w/v glucose and induced with 1.5 mM IPTG. The expression was performed overnight at 30 °C under argon sparging.

All the following manipulations were performed under strict anaerobic conditions in a glove box (Plas Labs) under a 5% hydrogen - 95% nitrogen atmosphere. All solutions were supplemented with 2-20 mM sodium dithionite and equilibrated with the glove box atmosphere before use.

Purification was obtained by affinity chromatography using Strep-Tactin Superflow high capacity cartridges (IBA) following the manufacturer's instructions. Protein concentration was assayed with the Bradford assay using bovine serum albumin as standard. The typical yield for both CaHydA WT and C298D was 1.7 mg pure protein/L culture. Hydrogenase activity assay was performed as previously described [40]; CaHydA WT samples had typically a specific activity of approximately 1356 µmol min^{-1} (mg protein)$^{-1}$; CaHydA C298D sample had typically a specific activity of approximately 660 µmol min^{-1} (mg protein)$^{-1}$. The specific activities were consistent with those of other recombinant [FeFe]-hydrogenases [2,40,43-45].

An homology model of the enzyme structure was built as previously described [40].

2.2 EPR spectroscopy

Purified enzymes were anaerobically concentrated and the buffer was exchanged to remove trace dithionite. 5% v/v glycerol was added to the solution. The oxidized sample was obtained by the addition of 3.1 mM thionine and the final protein concentration was 0.4 mM. The CO-treated sample was obtained by sparging the oxidized sample with CO twice for 30 seconds on ice. A sample of 60 µL was sealed into a quartz tube (Wilmad LabGlass) with internal diameter 2 mm. Continuous wave (CW) EPR spectra were recorded with a Bruker EMX spectrometer operating at X-band (9.47 GHz) equipped with a cylindrical cavity. All the spectra were recorded with 100 kHz field modulation, microwave power 10 mW, modulation amplitude 0.2 mT and temperature 77 K. No attempts were made to obtain absolute spin concentrations.

Pulse EPR experiments were performed at X-band (9.76 GHz) on an ELEXYS 580 Bruker spectrometer equipped with a liquid-helium cryostat from Oxford Inc. The magnetic field was measured by means of a Bruker ER035 M NMR gauss meter. The spectra were recorded at T = 15 K.

Electron-spin-echo (ESE) detected EPR experiments were carried out with the pulse sequence: $\pi/2-\tau-\pi-\tau-echo$. The mw pulse lengths $t_{\pi/2}$ = 16 ns and t_{π} = 32 ns and a τ value of 200 ns was used.

Hyperfine Sublevel Correlation (HYSCORE) experiments were carried out with the pulse sequence $\pi/2-\tau-\pi/2-t_1-\pi-t_2-\pi/2-\tau-echo$. The mw pulse lengths $t_{\pi/2} = t_{\pi}$ = 16 ns were used, with starting time 96 ns for t_1 and t_2, and time increment Δt = 16 ns (data matrix 250 × 250). The spectra were recorded with different τ values, specified in the figures caption. A four-step phase cycle was used to remove unwanted echoes. The time traces of the HYSCORE spectra were baseline corrected with a third-order polynomial, apodized with a Hamming window and zero filled. After two-dimensional Fourier transformation, the absolute value spectra were calculated. For all the pulse experiments a shot repetition rate of 0.5 kHz was used.

Field swept EPR and HYSCORE spectra were simulated using the Easyspin package [46].

2.3 FTIR spectroscopy

All the manipulations and the assembly of the transmission cell were performed under strict anaerobic conditions using a glove box (Belle Technology) under a pure nitrogen atmosphere. Purified samples were concentrated by ultrafiltration up to 0.9-1 mM using Amicon Ultra 0.5 mL 30K MWCO (Millipore). The various samples were obtained as follows: the “as purified” sample was acquired just after concentration without any other treatment (the buffer contains approximately 2 mM sodium dithionite as a purification residual); the thionine oxidized sample was obtained by the addition of 6.7 mM thionine; the hydrogen reduced sample was obtained by sparging the sample with H_2 twice for 1 minute on ice; the dithionite reduced sample was obtained by the addition of 16.7 mM fresh sodium dithionite for 1 minute; the CO inhibited sample was obtained by sparging the sample with carbon monoxide twice for 30 seconds on ice.

The spectra were acquired at room temperature using a Bruker Tensor 27 FT-IR spectrometer (Bruker Instruments). A transmission cell equipped with CaF_2 window and 50 µm pathlength (Specac) was used; the sample chamber was purged with pure nitrogen gas. Spectra were acquired with a resolution of 2 cm^{-1} accumulating 256 scans. The baseline correction was obtained using the Opus 6.0 software (Bruker Instruments) by the concave rubberband algorithm and manual refinement of the baseline.

3. Results:

3.1 CW and Pulse EPR spectroscopy

X-band EPR experiments were performed on the paramagnetic H_{ox} and H_{ox}-CO states of CaHydA *wild type* (WT) and C298D mutant in order to examine possible structural changes in the local geometry of the EPR active site upon mutagenesis.

Prior to EPR analysis, the CaHydA samples were oxidized with an excess of thionine in order to enrich for the H_{ox} state of the H-cluster. The oxidation treatment was necessary to remove overlapping signals typical of reduced $[2Fe\text{-}2S]^{+}$ centers [47-50], presumably arising from the [2Fe-2S] redox center of CaHydA (Fig. S1 in Supplementary Material).

It has to be noted that the oxidation by "auto-oxidation", as described for *Chlamydomonas reinhardtii* HydA1 [20], was not sufficient for CaHydA, because the presence of the accessory iron sulphur centers in the so-called F-domain are not completely oxidized by this process resulting in a background of paramagnetic signals that do not originate from the H-cluster.

The CW EPR spectra recorded for the oxidized WT protein and C298D mutant are reported in Figure 3. The EPR spectrum of the WT sample (Fig. 3a) is dominated by a rhombic signal with principal g values g_1 =2.0892, g_2 =2.0363, g_3 =1.9954. These values are in agreement with those reported for the oxidized form of the H-cluster (H_{ox} state) of other hydrogenases [3,17,19,20,28,37,51-54]. In Figure 3c the CW EPR spectrum of the oxidized sample after flushing with CO shows the presence of the axial signal ascribable to the inhibited state of the H-cluster (H_{ox}-CO), characterized by g values g_1 = 2.0755 and $g_2 = g_3$ = 2.0080, as already reported for other systems [30,34,52].

The CW EPR spectra related to the H_{ox} and H_{ox}-CO states of the thionine oxidized C298D mutant are reported in Figure 3b and 3d, respectively. For both states a clear analogy with the spectra of the WT protein can be observed, namely a rhombic pattern for the H_{ox} state and an axial signal for the H_{ox}-CO state, with g values matching those found for the WT protein (Table 1). The comparison of the CW EPR spectra shown in Figure 3 thus suggests that the local geometry of the paramagnetic [2Fe] sub-cluster is essentially unaltered upon the mutagenesis process for the C298D mutant.

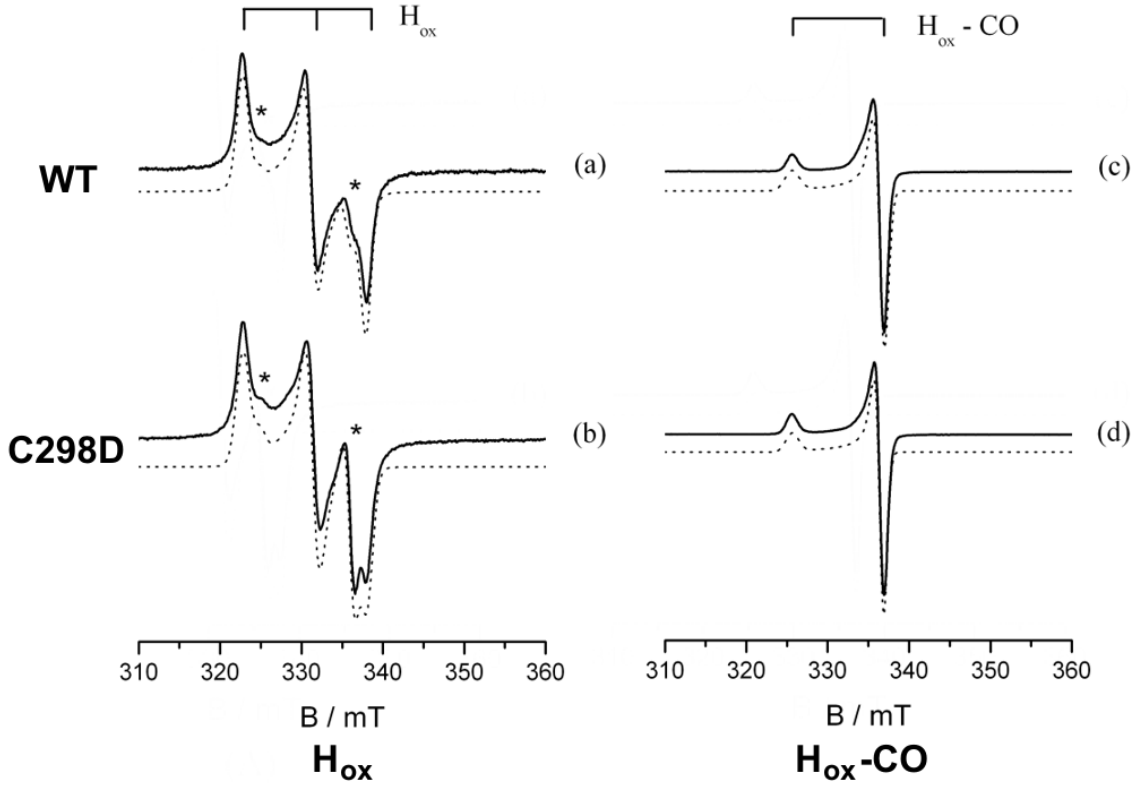

Figure 3. Experimental (solid lines) and computer simulated (dotted lines) X-band CW EPR spectra of the thionine oxidized CaHydA samples in the H_{ox} (left) and H_{ox}-CO (right) states of the H-cluster. Spectra (a), (c) refer to the WT protein and (b), (d) to the C298D mutant. The spin Hamiltonian parameters extracted from the computer simulations are reported in Table 1. The experimental spectra were recorded at T = 77 K. The stick diagrams on top of the spectra indicate the spectral features of the H_{ox} and H_{ox}-CO states. Asterisks in spectra (a) and (b) indicate the EPR pattern of the H_{ox}-CO state present as an impurity. **(2 columns fitting image).**

Further insights into the electronic structure of the active site and its chemical environment upon mutagenesis were obtained by extending the EPR investigation to pulse methods. For the present study HYSCORE experiments were performed at X-band in order to characterize both the H_{ox} and H_{ox}-CO states of the H-cluster of the oxidized WT and C298D mutant. The comparison between the HYSCORE spectra recorded for the two samples is reported in Figure 4 (see also Fig. S2 of the Supplementary Material). The spectra corresponding to the H_{ox} state (Fig. 4a and 4b) of the H-cluster show cross peaks stemming from the hyperfine interaction of the unpaired electron of the [2Fe] sub-cluster with nitrogen nuclei in both (+,+) and (-,+) quadrants. The computer simulation analysis of such nitrogen signals carried out on the spectra recorded at three magnetic field positions (Fig. S3 in Supplementary Material) allowed extracting the spin-Hamiltonian parameters

of the ^{14}N hyperfine and quadrupole couplings, which are listed in Table 2. In the simulation, one nitrogen nucleus was considered, whose hyperfine and quadrupole tensors are in line with those attributed to the CN ligand at the distal iron (Fe_d) site of the [2Fe] sub-cluster in DdH and CpI on the basis of the observed nuclear quadrupole interaction and comparison with DFT calculations [17,29,57]. The same ^{14}N signals have been observed for the C298D mutant, (Fig. 4b), clearly indicating a structural analogy in the CN ligand at the Fe_d site for the two systems in their H_{ox} state.

HYSCORE spectra recorded for the H_{ox}-CO state both CaHydA WT and C298D mutant (Fig. 4c and 4d), show cross peaks in the (+,+) quadrant due to the hyperfine interaction of the unpaired electron of the [2Fe] sub-cluster with nitrogen, carbon and proton nuclei. The spectra are similar to those reported by different authors for similar systems [28,30,58,59]. As in the case of the H_{ox} state, also for the H_{ox}-CO case the HYSCORE spectra of both WT and C298D mutant display nearly identical signals. A first set of cross peaks is centered along the (+,+) diagonal at about 3.7 MHz. The simulation analysis (Table 2) allowed ascribing this signal to double quantum transitions of a ^{14}N nuclear spin, as already reported for analogous HYSCORE spectra recorded for DdH [30]. The measured hyperfine interaction points to a weakly coupled ^{14}N nucleus with a large quadrupole interaction of 3.3 MHz, compatible with the nitrogen belonging to the CN ligand at the distal Fe of the [2Fe] sub-cluster in the H_{ox}-CO state [30].

Finally, an extended ridge centered at the proton Larmor frequency (ν_{1H} = 14.766 MHz at B_0 = 346.8 mT) is observed in the HYSCORE spectra of both the WT and the C298D mutant. The signal has a maximum extension of about 9 MHz consistent with previous observations for the H_{ox}-CO state of DdH [30] and of CpI [60]. Inspection of the ridge of the CaHydA samples reveals the presence of at least two proton signals, characterized by a different maximum extension (Fig. 4c and 4d). The computer simulation analysis performed at three field positions (Fig. S4 in Supplementary Material) allowed extracting the full hyperfine tensor for the two couplings, both dominated by the dipolar contribution (Table 2). Since several protons are present at distances compatible with the observed hyperfine couplings, a structural assignment is not possible at this stage.

To summarize, the comparison between the EPR and HYSCORE spectra recorded for CaHydA WT and C298D mutant indicates the absence of any significant structural and electronic modification of the H-cluster upon mutagenesis, suggesting that both the local geometry and the chemical environment of the active site are preserved.

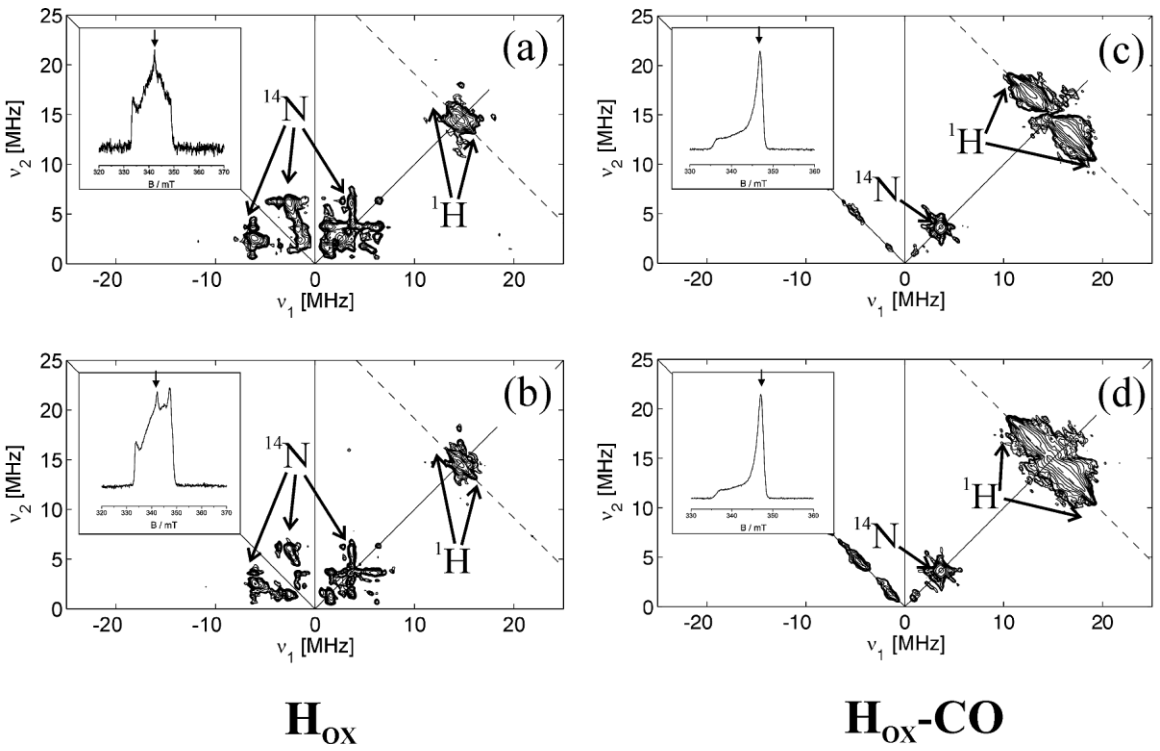

Figure 4. Experimental X-band HYSCORE spectra of the H_{ox} (left) and H_{ox}-CO (right) states of the thionine oxidized CaHydA. Spectra (a), (c) refer to the WT protein and (b), (d) to the C298D mutant. The spectra were recorded at field positions corresponding to (a) 341.6 mT, (b) 346.8 mT, (c) 342.2 mT and (d) 347.1 mT, as indicated by the arrow in the echo detected spectra in the insets. The τ values adopted for the experiments are: (a), (b) τ= 112 ns; for spectra (c), (d) two spectra recorded at τ = 136 and τ = 160 ns were summed together after Fourier transformation. All spectra were recorded at T = 15 K. The simulation analysis of the spectra is reported in the Supplementary Material (Fig. S3 and S4) and the corresponding spin Hamiltonian parameters are listed in Table 2. **(2 columns fitting image).**

3.2 FTIR spectroscopy

FTIR spectroscopy was used to investigate the structure of the H-cluster through the vibrational features of the CO and CN ligands under steady-state conditions (Fig. 5).

The spectrum of CaHydA WT without any treatment ("as purified") is complex and composed of a mixture of different redox states of the H-cluster. In order to dissect the various components, various oxidative and reductive treatments were applied.

When the WT enzyme was oxidized by thionine treatment, a much more homogeneous spectrum was obtained. The five major components of this spectrum (2082, 2070, 1969, 1946, 1801 cm^{-1}) can be associated with the spectra of previously studied [FeFe]-hydrogenases in their H_{ox} state and have been assigned to the five CO and CN ligands of the H-cluster (Table 3).

Reduction of the WT enzyme by H_2 resulted in the decrease of the H_{ox} signals and the increase of several other components (2063, 2053, 2040, 1989, 1937, 1920, 1899, 1893 cm^{-1}), that are also present in the "as purified" sample.

Reduction with dithionite gave a similar result, with few differences. In this case, the 1800 cm^{-1} peak was not detectable and the increase of the 1899 cm^{-1} was larger, while there was no proportionality in the increase of the 1937, 1920 and 1893 cm^{-1} signals; also, the signals at 2063 and 1989 cm^{-1} were absent.

The assignment of the signals observed in the reduced samples to a specific redox state and ligand is more complicated, because multiple bands were observed indicating a population of multiple states. Nevertheless, by differential spectroscopy (Fig. S5a and S5b in Supplementary Material) and a comparison with other [FeFe]-hydrogenases (Table 3) it is clear that the most intense signal at 1899 cm^{-1} can be assigned to the H_{red} state. This vibrational mode has been assigned to a shift of the bridging CO to a terminal position in H_{red} of DdH [33] and has also been observed in other [FeFe]-hydrogenases having a F-domain (such as CpI) [25]. However, this shift has not been observed in enzymes lacking these accessory redox centers (such as CrHydA1) [35]. Also the signals at 2053 and 2040 cm^{-1} can be assigned to the H_{red} state and to the cyanide ligands, while the assignment of the other signals remains ambiguous. Importantly, no signal was observed in the region around 1882-1883 cm^{-1}, which has been assigned to the H_{sred} state in DdH and CrHydA1 [34,35].

Treatment with CO generated an intense and homogeneous spectrum with six signals (2090, 2075, 2015, 1973, 1967, 1806 cm^{-1}) that are coherent with the expected peak shifts induced by the binding of exogenous CO at the Fe_d in the H_{ox}-CO state. All the signals can be assigned by comparison with the literature (Table 3) to the five endogenous ligands and the exogenous CO.

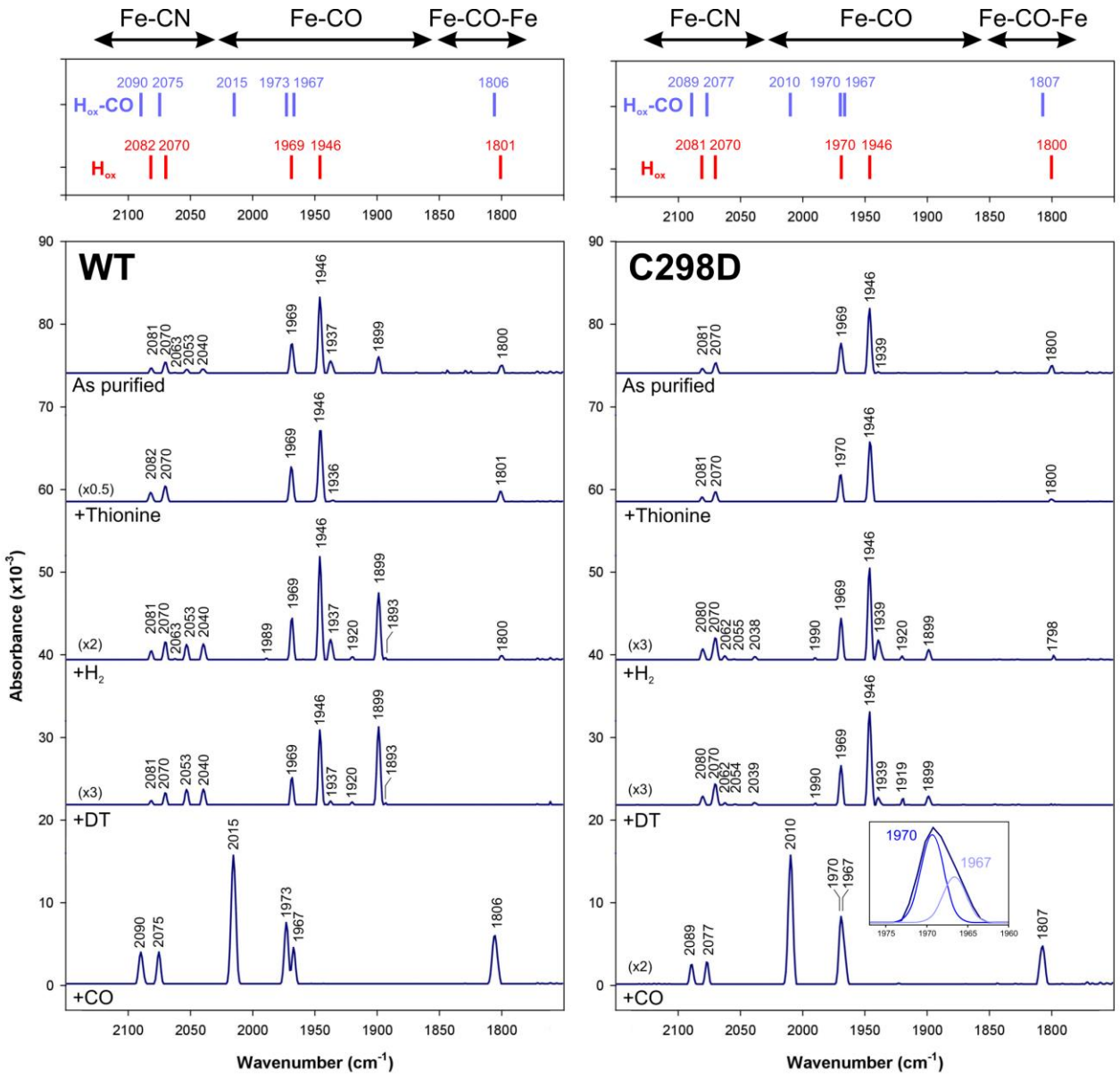

Figure 5. FTIR spectra under steady-state conditions acquired at room temperature. Left) CaHydA WT. Right) CaHydA C298D. The same conditions were used for the two enzymes: "as purified" was only concentrated without further treatment; thionine oxidation; H_2 reduced; dithionite reduced; CO inhibited. Note that some spectra have been scaled by the coefficient indicated in parentheses. For the assignments of the wavenumber to the H_{ox} and H_{ox}-CO states compare with the data in table 3. **(2 columns fitting image).**

The spectrum of the "as purified" CaHydA C298D is more homogeneous than the WT (Fig. 5). Also, the spectrum is almost identical after thionine oxidation, showing that the enzyme spontaneously equilibrates into the H_{ox} state even in the presence of 2 mM dithionite. Concerning the wavenumber of the signals, they are the same as the WT: the apparent small differences are not of significant relevance, considering the experimental spectral resolution.

Reduction with H_2 caused a decrease of the H_{ox} signals and the increase of various other peaks (2062, 2055, 2038, 1990, 1939, 1920, 1899 cm^{-1}). Reduction with dithionite caused a similar behaviour and the complete disappearance of the 1800 cm^{-1} peak. Under reducing conditions, excluding the H_{ox} signals, the most intense peaks were 1939 and 1899 cm^{-1}, in the region of the terminal COs, 2062 and 2038 cm^{-1} in the CNs region. The wavenumbers of these signals are the same as the WT, but the relative intensity is different especially in the CN region. Given the low intensity of the signals, the assignment of the peaks to a specific redox state and ligand is particularly difficult. Nevertheless, one interpretation is that the 1899 cm^{-1} signal correlates to the H_{red} state of the "semibridging" CO; by differential spectroscopy (Fig. S5c and S5d in Supplementary Material) and similar to the WT, signals at 2055 and 2038 cm^{-1} are assigned to CNs (Table 3).

Also, it is remarkable that the intensity of the H_{red} peaks in comparison to the H_{ox} was much weaker than in the WT; for example, the ratio between the 1899 cm^{-1} (H_{red}) and the 1946 cm^{-1} (H_{ox}) peaks is 0.65 for the H_2-reduced WT and only 0.11 for the C298D. Considering also that the signals of the H_{red} state are not present in the "as purified" state, these data suggest that the C298D mutant displays a difference in the equilibrium between the H_{ox} and the H_{red} states, that might be caused by a different mid-point redox potential of the transition and/or a difference in the balance between the oxidation/reduction kinetics of the H-cluster.

Treatment with CO caused the typical peak shifts, but apparently only five signals could be observed in the spectrum. However, a detailed analysis showed that the peak in the region 1960-1970 cm^{-1} was composed of two signals at 1970 cm^{-1} and 1967 cm^{-1}. In comparison to the WT, the cyanide and the bridging CO signals did not show a significant difference, while the region of the terminal COs was influenced. The peaks assigned to Fe_d shifted significantly, from 2015 and 1973 (WT) to 2010 and 1970 (C298D) cm^{-1}, while the peak assigned to Fe_p-CO was unaffected: 1967 cm^{-1}.

On the basis of the FTIR results, it is clear that the C298D mutation does not cause changes in the H-cluster geometry and environment when the enzyme is under its functional condition (*e.g.* the H_{ox} and H_{red} states); however, when the enzyme is inhibited by CO and the free coordination of Fe_d is occupied, slight modifications occur. These differences arise probably by the steric interaction of

the exogenous CO (a diatomic ligand) with the side chain of aspartic acid that is slightly bulkier than that of cysteine and that has a different charge distribution.

4. Discussion

In this work, the *wild type* [FeFe]-hydrogenase CaHydA was characterized for the first time by FTIR, CW and pulse EPR spectroscopies. Subsequently, the spectroscopic features of the WT enzyme were compared to the C298D mutant, in order to investigate in details the effect of such mutation on the H-cluster.

The characterisation of the WT enzyme showed features consistent with other [FeFe]-hydrogenases, both in the case of EPR and FTIR spectroscopies. A clear assignment of the H_{ox} and H_{ox}-CO signals was done, while given the presence of the accessory iron sulphur centers in the F-domain, the study of the reduced states was more complicated and no EPR experiments have been performed on these states.

The results presented here show that the electronic structure of the H-cluster is unaltered in the C298D mutant, as observed in CW and pulse EPR experiments, and that the vibrational modes of the CO and CN ligands are substantially unaffected, as observed in FTIR experiments. Remarkably, the signal positions were the same in the WT and C298D mutant in most redox states. The only significant difference in terms of signal position could be observed in the H_{ox}-CO state in FTIR spectra: the peaks assigned to the terminal COs are shifted to lower wavenumbers in C298D. This shift is probably caused by hindrance between the CO_{exo} and the side chain of aspartic acid, also affecting the adjacent Fe_d-CO and its interactions with the surrounding protein framework. This spectroscopic difference was only observed when the sixth coordination of Fe_d was occupied by exogenous CO; in this situation the difference in size and charge distribution between the side chains of cysteine (WT) and aspartic acid (C298D) becomes evident. This suggests that, even upon exogenous CO treatment, there is no structural change in the C298D mutant, but only fine modifications in the vibrational properties of the CO ligands occur.

The effects of mutations in the close proximity of the H-cluster have been spectroscopically studied only in few other cases [21,37]. In both cases the homologue of cysteine 298 was studied in CrHydA1: the mutation C169S, where cysteine was replaced by serine, a non-ionisable residue, caused either complete loss of activity [37] or an important activity decrease (30-40 fold) [21]. In both works the impairment of the proton transfer pathway to the H-cluster caused several spectroscopic differences in comparison to the WT, including the shift of the spectroscopic signals to other positions and the alteration of the steady-state equilibrium of the H-cluster.

In contrast, given the high catalytic activity of our C298D mutant (cysteine replacement with aspartic acid, an ionisable residue where the activity decrease was only 2 fold), the spectral differences in comparison with the WT enzyme were very small.

The replacement of cysteine with non-ionisable residues, such as serine, leads to impairment in the proton transfer and severely alters the catalysis by affecting the H-cluster reactivity [21], while the replacement with an ionisable residue, such as aspartic acid, can sustain catalytic activity at high rates because the proton transfer kinetics are influenced very little [40]. In fact, we did not observe the accumulation of a reduced intermediate with terminally bound H-species that slows down and prevents CO binding at the H-cluster; such an intermediate was suggested for the homologous serine mutant where the proton exchange between the H-cluster and the protein was severly altered [21].

A small impairement of optimal proton transfer kinetics is also expected in our experimental condition due to aspartic acid replacement and accounting for the decreased rates of enzyme activity. Although less pronounced than in the serine mutant the signature of this altered proton transfer is observed as an imbalance between the H_{ox}/H_{red} states, as the H_{red} signals in the FTIR spectra of the C298D mutant were proportionally lower than in the WT even when reductive treatments were applied. In the future, the determination of the mid-point potential of the two proteins might contribute to interpret this difference.

The very precise and fine tuning of the redox and kinetic equilibria in the hydrogenase catalytic cycle are clearly matching the stringent requirement selected by evolution of cysteine at position 298 (or homologous): although aspartate was demonstrated here to be a good substitute both in terms of structural integrity and of activity of the cluster, there is no evidence to date of any natural [FeFe]-hydrogenase [1,26] displaying such aminoacid at the key position for proton transfer between the H-cluster and the protein moiety.

5. Conclusions

In conjunction with previous works [21,37,39,40], our data enhance the importance of considering the H-cluster and its protein environment as a dynamic inseparable system that synergistically cooperates for an efficient and fast catalytic mechanism. The results presented here are required for the understanding of the [FeFe]-hydrogenases function in the perspective of an improvement for the exploitation in biotechnological applications [62,63], but also they must be considered when designing bio-inspired catalysts and mimics [26,63-67].

Acknowledgements

This work was supported by "RICERCA LOCALE" 2012 and 2013 from the University of Torino and, partially, by project HyStrEM (E.U. Structural Funds N.1083/2006 F.E.S.R. 2007-2013).

D.W.M., M.W.R., and P.W.K. gratefully acknowledge funding support for assistance with hydrogenase expression and FTIR data collection methods from the U.S. Department of Energy, Office of Science, Basic Energy Sciences, Division of Chemical Sciences, Geosciences, and Biosciences and support of the U.S. Department of Energy under contract no. DE-AC36-08-GO28308 with the National Renewable Energy Laboratory.

References:

1. P.M. Vignais, B. Billoud, Occurrence, Classification, and Biological Function of Hydrogenases: An Overview, Chem. Rev. 107 (2007) 4206-4272.
2. S. Kim, D. Lu, S. Park, G. Wang, Production of hydrogenases as biocatalysts, Int. J. Hydrogen Energy 37 (2012) 15833-15840.
3. W. Lubitz, H. Ogata, O. Rüdiger, E. Reijerse, Hydrogenases, Chem. Rev. 114 (2014) 4081-4148.
4. D.B. Levin, L. Pitt, M. Love, Biohydrogen production: prospects and limitations to practical application, Int. J. Hydrogen Energy 29 (2004) 173-185.
5. H.-S. Lee, W.F.J.; Vermaas, B.E. Rittmann, Biological hydrogen production: prospects and challenges, Trends Biotechnol. 28 (2010) 262-271.
6. M.C. Posewitz, P.W. King, S.L. Smolinski, L. Zhang, M. Seibert, M.L. Ghirardi, Discovery of Two Novel Radical S-Adenosylmethionine Proteins Required for the Assembly of an Active [Fe] Hydrogenase, J. Biol. Chem. 279 (2004) 25711–25720.
7. P. Berto, M. Di Valentin, L. Cendron, F. Vallese, M. Alberini, E. Salvatori, G.M. Giacometti, D. Carbonera, P. Costantini, The [4Fe–4S]-cluster coordination of [FeFe]-hydrogenase maturation protein HydF as revealed by EPR and HYSCORE spectroscopies, Biochim. Biophys. Acta 1817 (2012) 2149-2157.
8. Y. Nicolet, J.C. Fontecilla-Camps, Structure-Function Relationships in [FeFe]-Hydrogenase Active Site Maturation, J. Biol. Chem. 287 (2012) 13532-13540.
9. J.M. Kuchenreuther, W.K. Myers, T.A. Stich, S.J. George, Y. Nejatylahromy, J.R. Swartz, R.D. Britt, A Radical Intermediate in Tyrosine Scission to the CO and CN^- Ligands of FeFe Hydrogenase, Science 342 (2013) 472-475.
10. E.M. Shepard, F. Mus, J.N. Betz, A.S. Byer, B.R. Duffus, J.W. Peters, J.B. Broderick, [FeFe]-Hydrogenase Maturation, Biochemistry 53 (2014) 4090-4104.
11. J.W. Peters, W.N. Lanzilotta, B.J. Lemon, L.C. Seefeldt, X-ray Crystal Structure of the Fe-Only Hydrogenase (CpI) from *Clostridium pasteurianum* to 1.8 Angstrom Resolution, Science 282 (1998) 1853-1858.
12. Y. Nicolet, C. Piras, P. Legrand, E.C. Hatchikian, J.C. Fontecilla-Camps, *Desulfovibrio desulfuricans* iron hydrogenase: the structure shows unusual coordination to an active site Fe binuclear center, Structure 7 (1999) 13-23.
13. Y. Nicolet, B.J. Lemon, J.C. Fontecilla-Camps, J.W. Peters, A novel FeS cluster in Fe-only hydrogenases, Trends Biochem. Sci. 25 (2000) 138-143.

14. A.S. Pandey, T.V. Harris, L.J. Giles, J.W. Peters, R.K. Szilagyi, Dithiomethylether as a Ligand in the Hydrogenase H-Cluster, J. Am. Chem. Soc. 130 (2008) 4533-4540.
15. H.J. Fan, M.B. Hall, A Capable Bridging Ligand for Fe-Only Hydrogenase: Density Functional Calculations of a Low-Energy Route for Heterolytic Cleavage and Formation of Dihydrogen, J. Am. Chem. Soc. 123 (2001) 3828-3829.
16. J.C. Fontecilla-Camps, A. Volbeda, C. Cavazza, Y. Nicolet, Structure/Function Relationships of [NiFe]- and [FeFe]-Hydrogenases, Chem. Rev. 107 (2007) 4273-4303.
17. A. Silakov, B. Wenk, E.; Reijerse, W.; Lubitz, ^{14}N HYSCORE investigation of the H-cluster of [FeFe] hydrogenase: evidence for a nitrogen in the dithiol bridge, Phys. Chem. Chem. Phys. 11 (2009) 6592-6599.
18. G. Berggren, A. Adamska, C. Lambertz, T.R. Simmons, J. Esselborn, M. Atta, S. Gambarelli, J.M. Mouesca, E. Reijerse, W. Lubitz, T. Happe, V. Artero, M. Fontecave, Biomimetic assembly and activation of [FeFe]-hydrogenases, Nature 499 (2013) 66-70.
19. A. Adamska, A. Silakov, C. Lambertz, O. Rüdiger, T. Happe, E. Reijerse, W. Lubitz, Identification and Characterization of the "Super-Reduced" State of the H-Cluster in [FeFe] Hydrogenase: A New Building Block for the Catalytic Cycle?, Angew. Chem. Int. Ed. 51 (2012) 11458-11462.
20. D.W. Mulder, M.W. Ratzloff, E.M. Shepard, A.S. Byer, S.M. Noone, J.W. Peters, J.B. Broderick, P.W. King, EPR and FTIR Analysis of the Mechanism of H_2 Activation by [FeFe]-Hydrogenase HydA1 from *Chlamydomonas reinhardtii*, J. Am. Chem. Soc. 135 (2013) 6921-6929.
21. D.W. Mulder, M.W. Ratzloff, M. Bruschi, C. Greco, E. Koonce, J.W. Peters, P.W. King, Investigations on the Role of Proton-Coupled Electron Transfer in Hydrogen Activation by [FeFe]-Hydrogenase, J. Am. Chem. Soc. 136 (2014) 15394-15402.
22. V. Hajj, C.; Baffert, K. Sybirna, I. Meynial-Salles, P. Soucaille, H. Bottin, V. Fourmond, C. Léger, FeFe hydrogenase reductive inactivation and implication for catalysis, Energy Environ. Sci. 7 (2014) 715-719.
23. A. Adamska-Venkatesh, D. Krawietz, J. Siebel, K. Weber, T. Happe, E. Reijerse, W. Lubitz, New Redox States Observed in [FeFe] Hydrogenases Reveal Redox Coupling Within the H-Cluster, J. Am. Chem. Soc. 136 (2014) 11339-11346.
24. P. Chernev, C. Lambertz, A. Brünje, N. Leidel, K.G.V. Sigfridson, R. Kositzki, C.-H. Hsieh, S. Yao, R. Schiwon, M. Driess, C. Limberg, T. Happe, M. Haumann, Hydride Binding to the Active Site of [FeFe]-Hydrogenase, Inorg. Chem. 53 (2014) 12164-12177.

25. A.L. De Lacey, V.M. Fernández, Activation and Inactivation of Hydrogenase Function and the Catalytic Cycle: Spectroelectrochemical Studies, Chem. Rev. 107 (2007) 4304-4330.
26. M. Winkler, J. Esselborn, T. Happe, Molecular basis of [FeFe]-hydrogenase function. An insight into the complex interplay between protein and catalytic cofactor, Biochim. Biophys. Acta 1827 (2013) 974-985.
27. V. Fourmond, C. Greco, K. Sybirna, C. Baffert, P.-H. Wang, P. Ezanno, M. Montefiori, M. Bruschi, I. Meynial-Salles, P. Soucaille, J. Blumberger, H. Bottin, L. De Gioia, C. Léger, The oxidative inactivation of FeFe hydrogenase reveals the flexibility of the H-cluster, Nat. Chem. 6 (2014) 336-342.
28. A. Silakov, E.J. Reijerse, S.P.J. Albracht, E.C. Hatchikian, W. Lubitz, The Electronic Structure of the H-Cluster in the [FeFe]-Hydrogenase from *Desulfovibrio desulfuricans*: A Q-band ^{57}Fe-ENDOR and HYSCORE Study, J. Am. Chem. Soc. 129 (2007) 11447-11458.
29. W.K. Myers, T.A. Stich, D.L.M. Suess, J.M. Kuchenreuther, J.R. Swartz, R.D. Britt, The Cyanide Ligands of [FeFe] Hydrogenase: Pulse EPR Studies of ^{13}C and ^{15}N-Labeled H-Cluster, J. Am. Chem. Soc. 136 (2014) 12237-12240.
30. A. Silakov, B. Wenk, E. Reijerse, S.P.J. Albracht, W. Lubitz, Spin distribution of the H-cluster in the H_{ox}-CO state of the [FeFe] hydrogenase from *Desulfovibrio desulfuricans*: HYSCORE and ENDOR study of ^{14}N and ^{13}C nuclear interactions, J. Biol. Inorg. Chem. 14 (2009) 301-313.
31. T. Van Der Spek, A.F. Arendsen, R.P. Happe, S. Yun, K.A. Bagley, D.J. Stufkens, W.R. Hagen, S.P.J. Albracht, Similarities in the architecture of the active sites of Ni-hydrogenases and Fe-hydrogenases detected by means of infrared spectroscopy, Eur J. Biochem. 237 (1996) 629-634.
32. A.J. Pierik, M. Hulstein, W.R. Hagen, S.P.J. Albracht, A low-spin iron with CN and CO as intrinsic ligands forms the core of the active site in [Fe]-hydrogenases, Eur. J. Biochem. 258 (1998) 572-578.
33. Y. Nicolet, A.L. De Lacey, X. Vernède, V.M. Fernandez, E.C. Hatchikian, J.C. Fontecilla-Camps, Crystallographic and FTIR Spectroscopic Evidence of Changes in Fe Coordination Upon Reduction of the Active Site of the Fe-Only Hydrogenase from *Desulfovibrio desulfuricans*, J. Am. Chem. Soc. 123 (2001) 1596-1601.
34. W. Roseboom, A.L. De Lacey, V.M. Fernandez, E.C. Hatchikian, S.P.J. Albracht, The active site of the [FeFe]-hydrogenase from *Desulfovibrio desulfuricans*. II. Redox properties, light sensitivity and CO-ligand exchange as observed by infrared spectroscopy, J. Biol. Inorg. Chem. 11 (2006) 102-118.

35. A. Silakov, C. Kamp, E. Reijerse, T. Happe, W. Lubitz, Spectroelectrochemical Characterization of the Active Site of the [FeFe] Hydrogenase HydA1 from *Chlamydomonas reinhardtii*, Biochemistry 48 (2009) 7780-7786.
36. J.M. Kuchenreuther, S.J. George, C.S. Grady-Smith, S.P. Cramer, J.R. Swartz, Cell-free H-cluster Synthesis and [FeFe] Hydrogenase Activation: All Five CO and CN^- Ligands Derive from Tyrosine, PloS ONE 6 (2011) e20346.
37. P. Knörzer, A. Silakov, C.E. Foster, F.A. Armstrong, W. Lubitz, T. Happe, Importance of the Protein Framework for Catalytic Activity of [FeFe]-Hydrogenases, J. Biol. Chem. 286 (2012) 38341-38347.
38. T. Lautier, P. Ezanno, C. Baffert, V. Fourmond, L. Cournac, J.C. Fontecilla-Camps, P. Soucaille, P. Bertrand, I. Meynial-Salles, C. Léger, The quest for a functional substrate access tunnel in FeFe hydrogenase, Faraday Discuss. 148 (2011) 385-407.
39. A.J. Cornish, K. Gärtner, H. Yang, J.W. Peters, E.L. Hegg, Mechanism of Proton Transfer in [FeFe]-Hydrogenase from *Clostridium pasteurianum*, J. Biol. Chem. 286 (2011) 38341-38347.
40. S. Morra, A. Giraudo, G. Di Nardo, P.W. King, G. Gilardi, F. Valetti, Site Saturation Mutagenesis Demonstrates a Central Role for Cysteine 298 as Proton Donor to the Catalytic Site in CaHydA [FeFe]-Hydrogenase, PLoS ONE 7 (2012) e48400.
41. B. Ginovska-Pangovska, M.-H. Ho, J.C. Linehan, Y. Cheng, M. Dupuis, S. Raugei, W.J. Shaw, Molecular dynamics study of the proposed proton transport pathways in [FeFe]-hydrogenase, Biochim. Biophys. Acta 1837 (2014) 131-138.
42. H. Long, P.W. King, C.H. Chang, Proton Transport in *Clostridium pasteurianum* [FeFe] Hydrogenase I: A Computational Study, J. Phys Chem. B 118 (2014) 890-900.
43. P.W. King, M.C. Posewitz, M.L. Ghirardi, M. Seibert, Functional Studies of [FeFe] Hydrogenase Maturation in an *Escherichia coli* Biosynthetic System, J. Bacteriol. 188 (2006) 2163-2172.
44. J.M. Kuchenreuther, C.S. Grady-Smith, A.S. Bingham, S.J. George, S.P. Cramer, J.R. Swartz, High-Yield Expression of Heterologous [FeFe] Hydrogenases in Escherichia coli, PloS ONE 5 (2010) e15491.
45. I. Yacoby, L.T. Tegler, S. Pochekailov, S. Zhang, P.W. King, Optimized Expression and Purification for High-Activity Preparations of Algal [FeFe]-Hydrogenase, PloS ONE 7 (2012) e35886.
46. S. Stoll, A.J. Schweiger, EasySpin, a Comprehensive Software Package for Spectral Simulation and Analysis in EPR, Magn. Reson. 178 (2006) 42-55.

47. N. Hugo, J. Armengaud, J. Gaillard, K.N. Timmis, Y. Jouanneau, A Novel [2Fe-2S] Ferredoxin from *Pseudomonas putida* mt2 Promotes the Reductive Reactivation of Catechol 2,3-Dioxygenase, J. Biol. Chem. 273 (1998) 9622-9629.
48. G. Yakovlev, T. Reda, J. Hirst, Reevaluating the relationship between EPR spectra and enzyme structure for the iron–sulfur clusters in NADH:quinone oxidoreductase, Proc. Natl. Acad. Sci. 104 (2007) 12720-12725.
49. G. Mitou, C. Higgins, P. Wittung-Stafshede, R.C. Conover, A.D. Smith, M.K. Johnson, J. Gaillard, A. Stubna, E. Münck, J. Meyer, An Isc-Type Extremely Thermostable [2Fe-2S] Ferredoxin from *Aquifex aeolicus*. Biochemical, Spectroscopic, and Unfolding Studies, J. Biochemistry 42 (2003) 1354-1364.
50. S.A. Dikanov, R.I. Samoilova, R. Kappl, A.R Crofts, J. Hüttermann, The reduced [2Fe-2S] clusters in adrenodoxin and *Arthrospira platensis* ferredoxin share spin density with protein nitrogens, probed using 2D ESEEM, J. Phys. Chem. Chem. Phys. 11 (2009) 6807-6819.
51. B. Bennett, B.J. Lemon, J.W. Peters, Reversible Carbon Monoxide Binding and Inhibition at the Active Site of the Fe-Only Hydrogenase, Biochemistry 39 (2000) 7455-7460.
52. S.P.J. Albracht, W. Roseboom, E.C. Hatchikian, The active site of the [FeFe]-hydrogenase from *Desulfovibrio desulfuricans*. I. Light sensitivity and magnetic hyperfine interactions as observed by electron paramagnetic resonance, J. Biol. Inorg. Chem. 11 (2006) 88-101.
53. G. von Abendroth, S. Stripp, A. Silakov, C. Croux, P. Soucaille, L. Girbal, T. Happe, Optimized over-expression of [FeFe] hydrogenases with high specific activity in *Clostridium acetobutylicum*, Int. J. Hydrogen Energy 33 (2008) 6076-6081.
54. C. Kamp, A. Silakov, M. Winkler, E.J. Reijerse, W. Lubitz, T. Happe, Isolation and first EPR characterization of the [FeFe]-hydrogenases from green algae, Biochim. Biophys. Acta 1777 (2008) 410-416.
55. M.W.W. Adams, The Mechanisms of H_2 Activation and CO Binding by Hydrogenase I and Hydrogenase II of *Clostridium pasteurianum*, J. Biol. Chem. 262 (1987) 15054-15061.
56. S. Morra, B. Mongili, S. Maurelli, G. Gilardi, F. Valetti, Isolation and Characterization of a New [FeFe]-Hydrogenase from *Clostridium perfringens*, Biotechnol. Appl. Biochem. (2015) in press doi: 10.1002/bab.1382.
57. A. Adamska-Venkatesh, T.R. Simmons, J.F. Siebel, V. Artero, M. Fontecave, E. Reijerse, W. Lubitz, Artificially maturated [FeFe] hydrogenase from *Chlamydomonas reinhardtii*: a HYSCORE and ENDOR study of a non-natural H-cluster, Phys. Chem. Chem. Phys. 17 (2015) 5421-5430.

58. C.V. Popescu, E. Münck, Electronic Structure of the H Cluster in [Fe]-Hydrogenases, J. Am. Chem. Soc. 121 (1999) 7877-7884.
59. C. Greco, A. Silakov, M. Bruschi, U. Ryde, L. De Gioia, W. Lubitz, Magnetic Properties of [FeFe]-Hydrogenases: A Theoretical Investigation Based on Extended QM and QM/MM Models of the H-Cluster and Its Surroundings, Eur. J. Inorg. Chem. (2011) 1043-1049.
60. J. Telser, M.J. Benecky, M.W. Adams, L.E. Mortenson, B.M. Hoffman, An EPR and electron nuclear double resonance investigation of carbon monoxide binding to hydrogenase I (bidirectional) from *Clostridium pasteurianum* W5, J. Biol. Chem. 261 (1986) 13536-13541.
61. Z. Chen, B.J. Lemon, S. Huang, D.J. Swartz, J.W. Peters, K.A. Bagley, Infrared Studies of the CO-Inhibited Form of the Fe-Only Hydrogenase from *Clostridium pasteurianum* I: Examination of Its Light Sensitivity at Cryogenic Temperatures, Biochemistry 41 (2002) 2036-2043.
62. P.W. King, Designing interfaces of hydrogenase–nanomaterial hybrids for efficient solar conversion, Biochim. Biophys. Acta 1827 (2013) 949-957.
63. T. Happe, A. Hemschemeier, Metalloprotein mimics – old tools in a new light, Trends Biotechnol. 32 (2014) 170-176.
64. S. Groysman, R.H. Holm, Biomimetic Chemistry of Iron, Nickel, Molybdenum, and Tungsten in Sulfur-Ligated Protein Sites, Biochemistry 48 (2009) 2310-2320.
65. A.M. Kluwer, R. Kapre, F. Hartl, M. Lutz, A.L. Spek, A.M. Brouwer, P.W.N.M. van Leeuwen, J.N.H. Reek, Self-assembled biomimetic [2Fe2S]-hydrogenase-based photocatalyst for molecular hydrogen evolution, Proc. Natl. Acad. Sci. 106 (2009) 10460-10465.
66. M. Faiella, A. Roy, D. Sommer, G. Ghirlanda, De Novo Design of Functional Proteins: Toward Artificial Hydrogenases, Biopolymers 100 (2013) 558-571.
67. M. Zhao, H.-B. Wang, L.-N. Ji, Z.-W. Mao, Insights into metalloenzyme microenvironments: biomimetic metal complexes with a functional second coordination sphere, Chem. Soc. Rev. 42 (2013) 8360-8375.

Tables and captions:

Table 1. Spin-Hamiltonian parameters of the H_{ox} and H_{ox}-CO states of H-cluster extracted by the computer simulations of the CW EPR spectra reported in Figure 3 in comparison with selected data from the literature.

Enzyme	H_{ox} state			H_{ox}-CO state			Ref.
	g_1	g_2	g_3	g_1	g_2	g_3	
CaHydA WT	2.0892 ±0.0005	2.0360 ±0.0005	1.9954 ±0.0005	2.0750 ±0.0005	2.007 ±0.005	2.007 ±0.005	This work
CaHydA C298D	2.0892 ±0.0005	2.0360 ±0.0005	1.9954 ±0.0005	2.0750 ±0.0005	2.007 ±0.005	2.007 ±0.005	This work
CaHydA	nd	nd	nd	2.075	2.009	2.009	53
CpI	2.098	2.040	2.001	2.074	2.011	2.011	55
CpHydA	2.0892	2.0363	1.9954	2.0755	2.008	2.008	56
DdH	2.10	2.04	2.00	2.06	2.00	2.00	52
	2.100	2.040	1.998	2.065	2.007	2.001	51
	2.100	2.040	1.997	2.065	2.007	2.001	17
CrHydA1	2.102	2.040	1.998	2.052	2.007	2.007	54
	2.10	2.037	1.996	2.052	2.007	2.007	19
	2.100	2.039	1.997	2.045	2.007	2.007	20
CsHydA	2.100	2.040	1.998	2.056	2.008	2.008	54
CmHydA1	2.103	2.038	1.998	2.050	2.008	2.008	54

Table 2. ^{14}N and ^{1}H hyperfine and quadrupole couplings deduced from the simulation analysis of the HYSCORE spectra of the H_{ox} and H_{ox}-CO states of H-cluster for both the thionine oxidized WT CaHydA protein and the C298D mutant of Figure 4. The computer simulations are reported in Figures S3 and S4 of the Supplementary Material section. The coupling constants are given in MHz, the Euler angles are in degree. Comparison is made with the signals reported in the literature for other hydrogenases.

	Species	**H-cluster state**	A_x	A_y	A_z	**α, β, γ**	e^2qQ/h	**η**	**α',β',γ'**	**Ref.**
^{14}N	CaHydA	H_{ox}	1.5 ±0.1	3.9 ±0.1	-0.4 ±0.1	30±10, 30±10, 0±10	3.7 ±0.1	0.3 ±0.05	0±10, 40±10, 0±10	This work
^{14}N (CN at Fe_d)		H_{ox}	1.5	3.8	-0.4	41,34,0	3.84	0.34	-26,24,0	
^{14}N (DTMA)	DdH	H_{ox}	1.0	1.9	1.4	40, 25, 0	4.92	0.13	10, 0, 0	17
^{14}N (Lys)		H_{ox}	-2.4	1.4	-0.7	0, 4, 20	1.44	0.80	147, 56, 0	
^{14}N (CN at Fe_d)	CpI	H_{ox}	0.6	4.5	-0.8	45, -20, 0				29
^{14}N	CaHydA	H_{ox}-CO	0.4 ±0.1	-0.2 ±0.1	0.6 ±0.1	20±10, -10±10, 0±10	3.3 ±0.1	0.6 ±0.1	50±20, 50±20, 0±10	This work
^{14}N (CN at Fe_d)	DdH	H_{ox}-CO	0.4	-0.2	0.56	0, -10, 0	3.04	0.64	0, 30, 0	30
^{1}H	CaHydA	H_{ox}-CO	-2.5 ±0.2	-2.5 ±0.2	9.5 ±0.5	0±10, 80±10, 0±10	-	-	-	This work
			-2.0 ±0.2	-2.0 ±0.2	5.0 ±0.2	0±10, 80±10, 0±10	-	-	-	

Table 3. Summary of FTIR wavenumbers of CaHydA WT and C298D in comparison with other [FeFe]-hydrogenases from the literature in various redox states.

Enzyme	H_{ox} state				Ref.
	CNs	Fe_p-CO	Fe_d-CO	μ-CO	
CaHydA WT	2082, 2070	1969	1946	1801	This work
CaHydA C298D	2081, 2070	1970	1946	1800	This work
CpI	2086, 2072	1971	1948	1802	61
CpHydA	2087, 2080	1968	1944	1800	56
DdH	2093, 2079	1965	1940	1802	34
CrHydA1 WT	2088, 2072	1964	1940	1800	35

Enzyme	H_{ox}-CO state					
	CNs	Fe_p-CO	Fe_d-CO	CO_{exo}	μ-CO	
CaHydA WT	2090, 2075	1967	1973	2015	1806	This work
CaHydA C298D	2089, 2077	1967	1970	2010	1807	This work
CpI	2095, 2077	1971	1974	2017	1810	61
CpHydA	2091, 2088	1967	1971	2013	1806	56
DdH	2096, 2088	1963	1971	2016	1810	34
CrHydA1 WT	2092, 2084	1964	1970	2013	1810	35

Enzyme	H_{red} state		
	CNs	COs	
CaHydA WT	2053, 2040	1899	This work
CaHydA C298D	2055, 2038	1899	This work
CpHydA	2066, 2039	1897	56
DdH	2079, 2041	1965, 1916, 1894	34
CrHydA1 WT	2083, 2070	1935, 1891, 1793	35